Hydrothermal Conversion of Zeolites: An *in Situ* Synchrotron X-ray Powder Diffraction Study

P. Norby*

Contribution from the Chemistry Department, Brookhaven National Laboratory, Upton, New York, 11973

Received December 9, 1996[⊗]

Abstract: Hydrothermal conversion of zeolite LTA by LiCl$_{(aq)}$ is an efficient synthesis route for zeolite Li-A(BW), LiAlSiO$_4$·H$_2$O, resulting in highly crystalline materials. In the present work hydrothermal crystallization of zeolite Li-A(BW) was followed *in situ* by time resolved synchrotron X-ray powder diffraction. These experiments were combined with *ex situ* scanning electron microscopy on partially converted samples. Fitting of the crystallization curves with rate expressions indicated limited nucleation and showed that intermediate amorphous or solute phases were not present in any significant amount. Partially converted samples were prepared *in situ*, making it possible to monitor the progress of crystallization and to determine the degree of conversion in each sample. Scanning electron microscope images of 40 and 60% converted samples showed that the parent zeolite LTA crystallites to a large degree serve as nucleation centers for the crystallization of zeolite Li-A(BW). The zeolite Li-A(BW) crystals grow radially from the nucleation site, forming clusters of flat needle-like crystals. The information obtained from the combined experiments clearly shows that the hydrothermal conversion of zeolite LTA into zeolite Li-A(BW) is a solution-mediated process.

Introduction

Zeolites are crystalline microporous materials which are of considerable technological interest in connection with, e.g., catalysis, adsorption, ion conductivity, and ion exchange. A large number of zeolite type materials have been prepared with a variety of properties and chemical compositions.

Zeolites and zeolite-like materials have crystallographically ordered and well-defined pores and cages of molecular dimensions in which water molecules and charge compensating cations are situated. The structure, shape, and chemical composition of pores and cages are important as for instance catalytic reactions take place on the inner surface of the material. Likewise, the nature and position of extra-framework charge compensating cations play an important role in determining the properties. Therefore, synthesis of new zeolitic materials designed with specific properties is a major research area, and an understanding of syntheses mechanisms etc. is a requirement for targeted materials design.

Conventionally, hydrothermal syntheses of aluminosilicate zeolites are performed under alkaline conditions with use of an amorphous aluminosilicate gel as the starting material. An alternative route for synthesizing zeolitic or aluminosilicate materials is conversion of zeolites under hydrothermal conditions.[1] This method has been little studied, although Barrer describes the variety of zeolites and aluminosilicates obtainable from hydrothermal conversion of analcite and leucite with different reaction conditions.[2,3] Studies of conversion of zeolite LTA into hydroxysodalite and zeolite P also have been

reported.[4,5] Some of the materials, which can be synthesized via hydrothermal conversion, are not obtainable by direct synthesis with conventional hydrothermal methods. Although most of the hydrothermal conversion syntheses reported have been performed in alkaline solutions, one of the advantages compared to conventional hydrothermal zeolite synthesis is that syntheses can be performed in solutions with pH close to neutral. Direct synthesis of, for instance, silver zeolites with conventional hydrothermal synthesis is not feasible in alkaline solutions. However, by hydrothermal conversion of zeolite LTA with AgNO$_{3(aq)}$, direct synthesis of Ag/NO$_3$-cancrinite is possible in neutral solutions.[6]

Hydrothermal conversion of zeolite LTA with an aqueous solution of LiCl at temperatures from 180 to 350 °C results in formation of zeolite Li-A(BW), LiAlSiO$_4$·H$_2$O.[1] Zeolite Li-A(BW) also can be obtained from amorphous aluminosilicate gels by conventional hydrothermal synthesis.[7] However, hydrothermal conversion of zeolite LTA is an easy and convenient method for obtaining pure and highly crystalline zeolite Li-A(BW), and it is of interest to obtain information about the crystallization mechanism.

In situ time resolved X-ray powder diffraction is becoming an efficient method for following hydrothermal synthesis of zeolites and gaining information concerning crystallization kinetics, formation of intermediate phases, and structural transitions. When taking advantage of high-intensity synchrotron X-ray radiation combined with position-sensitive detectors,[8−11] even relatively fast chemical reactions can be followed with a time resolution on the order of seconds. When studying

* Address correspondence to the following address: Department of Chemistry, State University of New York at Stony Brook, Stony Brook, NY, 11794.

⊗ Abstract published in *Advance ACS Abstracts,* May 15, 1997.

(1) Norby, P.; Nørlund Christensen, A.; Krogh Andersen, I. G. *Acta Chem. Scand.* **1986,** *A40*, 500−506.

(2) Barrer, R. M.; Hinds, L.; White, E. A. *J. Chem. Soc.* **1955,** 1466−1475.

(3) Barrer, R. M. *Hydrothermal Chemistry of Zeolites*; Academic Press: London, 1982.

(4) Subotić, B.; Mašić, N.; Šmit, I. In *Zeolites*; Elsevier: Amsterdam, 1985, pp 207−214.

(5) Subotić, B.; Šmit, I.; Madžija, O.; Sekovanić, L. *Zeolites* **1982,** *2*, 135−142.

(6) Norby, P. Unpublished results.

(7) Barrer, R. M.; White, E. A. *J. Chem. Soc.* **1951,** 1267−1278.

(8) Norby, P. *Mater. Sci. Forum* **1996,** *228−231*, 147−152.

(9) Norby, P.; Nørlund Christensen, A.; Hanson, J. C. In *Stud. Surf. Sci. Catal.* **1994,** *84*, 179−186.

(10) Gualtieri, A.; Norby, P.; Artioli, G.; Hanson, J. C. *Phys. Chem. Miner.* **1997,** *24*, 191−199.

hydrothermal syntheses the pressure inside the reaction vessel must be equal to or higher than the vapor pressure of the reaction mixture at the given temperature in order to maintain hydrothermal conditions. This can be achieved with autogenous pressure created by heating the whole reaction vessel (70−80% filled). This technique has been used for *in situ* studies of hydrothermal syntheses with energy dispersive diffraction.[12−15] An alternative approach is to apply an external pressure to the reaction mixture. When this method is used it is not necessary to heat the whole vessel. We have used the latter approach for *in situ* studies of hydrothermal syntheses and hydrothermal conversion of zeolites and related materials with angular dispersive powder diffraction.[8−11]

In the present work *in situ* synchrotron X-ray powder diffraction studies of hydrothermal conversion of zeolite LTA were combined with *ex situ* scanning electron microscopy (SEM). Partially converted samples were prepared *in situ* on the diffractometer, and the progress of crystallization and degradation was investigated with SEM.

Experimental Section

The materials used were zeolite Na-LTA ($Na_{12}Al_{12}Si_{12}O_{48}\cdot27H_2O$, Union Carbide) and LiCl (Merck, p.a.). Partially Li-exchanged zeolite, LTA (Li/Na-LTA), was prepared by ion exchange in a 2 M aqueous LiCl solution for 24 h at room temperature. Slurries (pH ∼8) were prepared by mixing 0.5 g of zeolite (Na-LTA or Li/Na-LTA) and 0.5 g of LiCl in 1.6 mL of demineralized water. The slurries were filled into 0.7 mm quartz glass capillaries by using a 0.5 mm capillary mounted on a syringe.

In situ powder diffraction studies were performed with use of synchrotron X-ray radiation at the Brookhaven Chemistry Department Beamline X7B at NSLS. We have developed equipment at the beamline for time-resolved *in situ* studies of hydrothermal synthesis,[8,9] where hydrothermal conditions at temperatures up to 260 °C can be obtained.

Samples were contained in 0.7 mm quartz glass capillaries mounted in a Swagelock fitting with a Vespel ferrule as shown in Figure 1. This setup, using an open capillary with gas flow, has been used also for time-resolved studies of catalysts under operating conditions.[17] When used for *in situ* studies of hydrothermal syntheses the capillary is closed and filled with the reaction mixture or gel using a thinner capillary mounted on a syringe. This allows pressure from e.g. an N_2 cylinder to be applied to the surface of the reaction mixture. Using a hot air stream, part of the reaction mixture is heated as shown in Figure 1, and the applied pressure ensures that hydrothermal conditions are obtained in the heated zone of the capillary. By heating only part of the reaction mixture, evaporation is suppressed because of the low temperature of the N_2-solution boundary. The heated zone was approximately 5 mm, while the X-ray beam was defined by slits to be 2 mm wide and 0.7 mm high. The width of the X-ray beam was kept much smaller than the heated zone in order to limit temperature gradients across the beam, as well as to reduce problems with transport of material by convection and diffusion. To minimize effects from
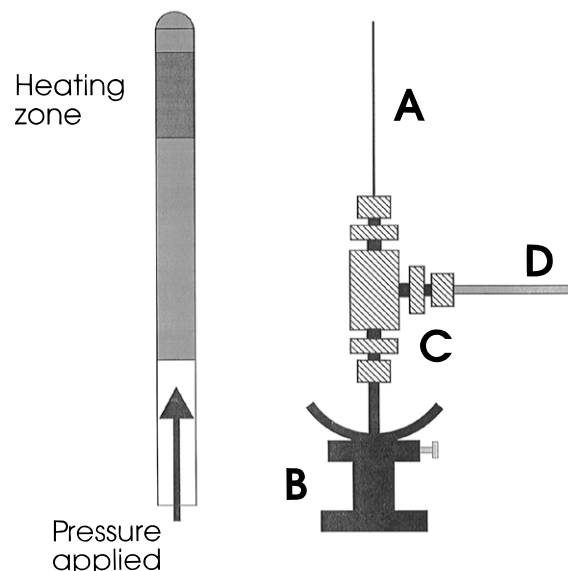

Figure 1. Sketch showing the quartz glass capillary (A) mounted on a goniometer head (B) with a Swagelock T-piece (C). A nitrogen pressure can be applied through the connected tubing (D). An exploded view of the capillary is shown to the left.

preferred orientation and to ensure random orientation of the crystallites, the sample was oscillated through an angle of 90°.

The maximum temperature is limited by the pressure that can be applied inside the capillary and by chemical reactions with the quartz glass. Standard 0.5-mm quartz glass capillaries (wall thickness 0.01 mm) usually can withstand an internal pressure of up to 50−60 atm, although this limit does depend on the quality of the individual capillary. Quartz glass is relatively chemically inert, but will react and weaken after prolonged exposure to alkaline solutions or gels at higher temperatures.

The detector used for collecting the powder diffraction patterns was a Translating Image Plate (TIP) camera constructed especially for time-, temperature-, and wavelength-dependent powder diffraction experiments.[8,18] A 200 × 400 mm Fuji imaging plate is translated horizontally behind a steel screen with a 3-mm vertical slit. A continuous series of powder diffraction patterns is thereby recorded. The large dynamic range obtained with imaging plates allows very good intensity data to be extracted from the image, making Rietveld refinement of time-resolved powder diffraction data possible.[19,20] The wavelength, sample-detector distance, zero point, and imaging plate tilt were determined from a LaB_6 standard (NIST #660) as described in ref 19.

The progress of crystallization and degradation was estimated from the TIP images by using integrated intensities of diffraction lines. The individual pixel size of the imaging plate is 0.1 × 0.1 mm, and the imaging plate was divided into 1.5 mm wide diffraction patterns by adding 15 pixels. Well-resolved diffraction lines with no overlap between the two phases were used (Zeolite LTA: 002, 022 (at positive and negative 2θ) and 222; Zeolite Li-A(BW): 110 and 121). A 2θ range was defined around each diffraction peak, and a linear background was defined by using background counts on each side of the peak. The background counts were subtracted from the total counts over the 2θ range to give the net integrated intensity. The integrated intensities of the selected reflections from each phase were added and normalized to represent the percentage of crystallinity. In the experiments with partial conversion, the intensities of the diffraction peaks of zeolite Li-A(BW) were normalized so that the final crystallinity of zeolite LTA and A(BW) added up to 100%. The intensities were corrected for decrease and fluctuations in the X-ray beam intensity by using monitor counts collected between the incident beam defining slit and the sample. The intensities were not corrected for image decay, which may cause

(11) Barnes, P.; Turrillas, X.; Jupe, A. C.; Colston, S. L.; O'Connor, D.; Cernik, R. J.; Livesey, P.; Hall, C.; Bates, D.; Dennnis, R. *J. Chem. Soc., Faraday Trans.* **1996**, *92*, 2187−2196.

(12) O'Hare, D.; Clark, S. M.; Evans, J. S. O.; Wong, H.-V. *Rev. Sci. Instrum.* **1995**, *66*, 2442−2445.

(13) Clark, S. M.; Nield, A.; Rathbone, T.; Flaherty, J.; Tang, C. C.; Evans, J. S. O.; Francis, R. J.; O'Hare, D. *Nucl. Instrum. Methods Phys. Res., Sect. B* **1995**, *97*, 98−101.

(14) Clark, S. M.; Cernik, R. J.; Grant, A.; York, S.; Atkinson, P. A.; Gallagher, A.; Stokes, D. G.; Gregory, S. R.; Harris, N.; Smith, W.; Hancock, M.; Miller, M. C.; Ackroyd, K.; Farrow, R.; Frances, R.; O'Hare, D. *Mater. Sci. Forum* **1996**, *228*, 213−217.

(15) Francis, R. J.; Price, S. J.; Evans, J. S. O.; O'Brien, S.; O'Hare, D.; Clark, S. M. *Chem. Mater.* **1996**, *8*, 2102−2108.

(16) Artioli, G.; Ståhl, K.; Hanson, J. C. *Mater. Sci. Forum* **1996**, *228−231*, 369−374.

(17) Clausen, B. S.; Steffensen, G.; Fabius, B.; Villadsen, J.; Feidenhans'l, R.; Topsoe, H. *J. Catal.* **1991**, *132*, 524−535.

(18) Norby, P.; Darovsky, A.; Hanson, J. C.; Meshkovsky, I. In preparation.

(19) Norby, P. *J. Appl. Crystallogr.* **1997**, *30*, 21−30.

(20) Gualtieri, A.; Norby, P.; Hanson, J. C.; Hriljac, J. *J. Appl. Crystallogr.* **1996**, *29*, 707−713.
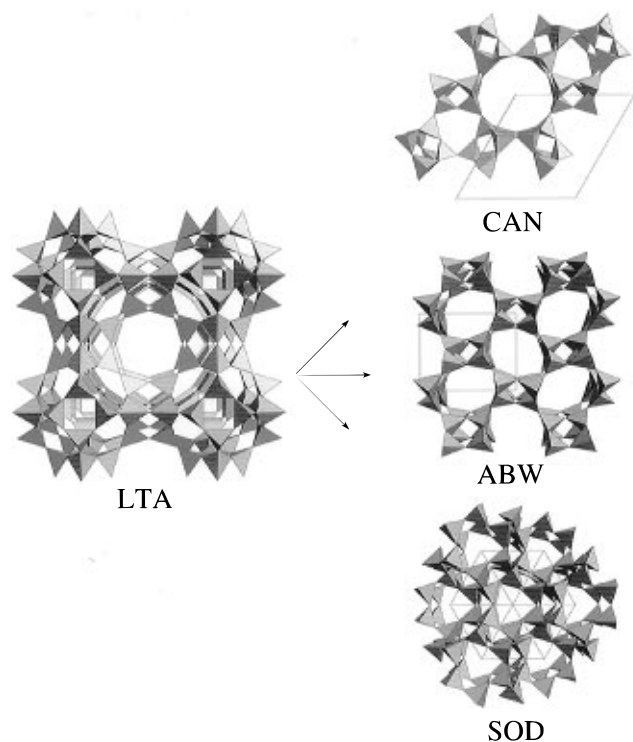
Figure 2. Tetrahedral representation of the framework structures of the starting material, LTA (cubic), and the three products obtained via hydrothermal conversion: sodalite (SOD, cubic), zeolite Li-A(BW) (ABW, orthorhombic), and cancrinite (CAN, hexagonal). Only the (Al,-Si)O$_4$ framework tetrahedra are shown in this figure. Extra-framework cations and water molecules are situated in the channels and cages of the zeolites.

systematic errors in intensities. The effect of the decay can in most cases be neglected if the imaging plates are not scanned immediately after the end of an experiment. The estimated standard deviation of the integrated intensities is between 0.2 and 1.5%, based on counting statistics. The major cause of uncertainty in intensity comes from variations in the translation speed of the imaging plate, observed as ripples on the crystallization curves.

Scanning electron microscopy (SEM) pictures were obtained with a Phillips XL-40/604 electron microscope. The samples for SEM were extracted from the heated zone of the capillaries after the crystallization

experiment. The obtained material was washed with demineralized water and dried.

Results

Three products were obtained in the thermal transformation of zeolite LTA with aqueous LiCl. Zeolite Li-A(BW), LiAlSiO$_4$·H$_2$O, was readily obtained at temperatures above 200 °C, as described earlier.[1] However, two phases were obtained which were not observed in the previous study. Figure 2 shows the tetrahedral framework structures of the starting material, zeolite A (LTA), and the products, zeolite Li-A(BW) (ABW), sodalite (SOD), and cancrinite (CAN).

In a previous study highly crystalline LiX-sodalites (X = Cl, Br) were prepared, but in an indirect way. NaX-sodalites (X = Cl, Br, I) are easily prepared by hydrothermal conversion of zeolite LTA with aqueous solutions of the sodium halides. LiCl and LiBr-sodalite were then obtained by hydrothermal ion exchange.[1] In the present study, however, LiCl-sodalite was formed in some experiments directly by hydrothermal conversion of zeolite LTA. The factors determining whether zeolite Li-A(BW) or LiCl-sodalite is formed are the solid/solution and solid/LiCl ratios. When the water content is high, zeolite Li-A(BW) is formed, while the formation of LiCl-sodalite is favored by low water contents. This is understandable as the zeolite framework is stabilized by water molecules, while sodalite is stabilized by the occluded salt.

Another phase formed is a material with a diffraction pattern indicating a cancrinite type material. Formation of salt bearing cancrinite is usually favored by CO$_3^{2-}$ or NO$_3^-$ anions,[21] which are not present here. However, cancrinite is also obtained in mixed-cation environments, especially when a large and a small cation are present.[22,23] Thus the material synthesized may be a mixed Li/Na-cancrinite. This is supported by the experiments with hydrothermal conversion of a Li-exchanged zeolite LTA, where the amount of sodium cations present was significantly reduced. In these syntheses formation of the cancrinite-like phase was significantly reduced. Another way of decreasing the amount of cancrinite formed is by using a higher water content, in which case pure zeolite Li-A(BW) is obtained.

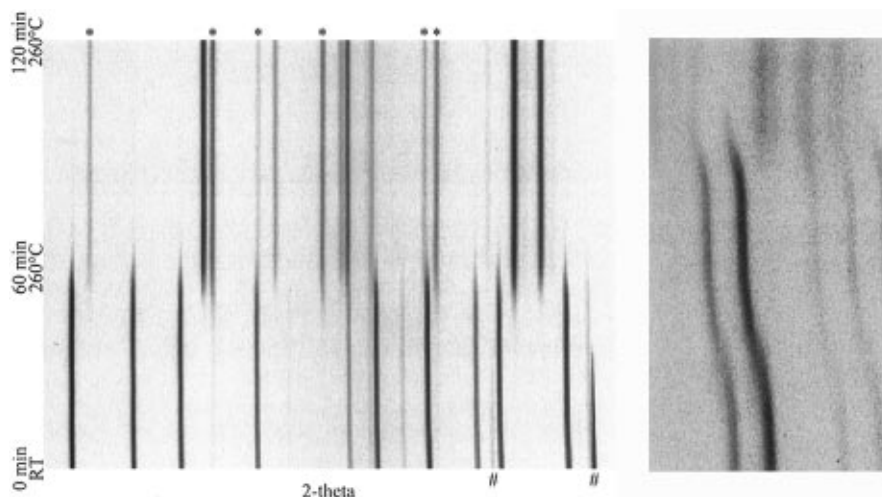Figure 3a is an example of a TIP image showing the hydrothermal conversion of zeolite LTA with an aqueous

Figure 3. (a, left) Part of a time resolved powder diffraction image collected with the Translating Imaging Plate Camera, wavelength 1.2571(5) Å. Hydrothermal conversion of zeolite Sodium-LTA in LiCl$_{(aq)}$ was performed by ramping the temperature from 25 °C to 260 °C in 1 h and holding the temperature constant for 1 h. The pressure applied was 45 atm. Diffraction peaks from LiCl (marked by #) disappear as LiCl is dissolved at higher temperatures. The product is a mixture of zeolite Li-A(BW) and a cancrinite type phase. Diffraction peaks from the cancrinite phase are marked with asterisks. (b, right) Enlargement of a small part of the image from part a at higher angles showing changes in the LTA diffraction pattern preceding the conversion to zeolite Li-A(BW).
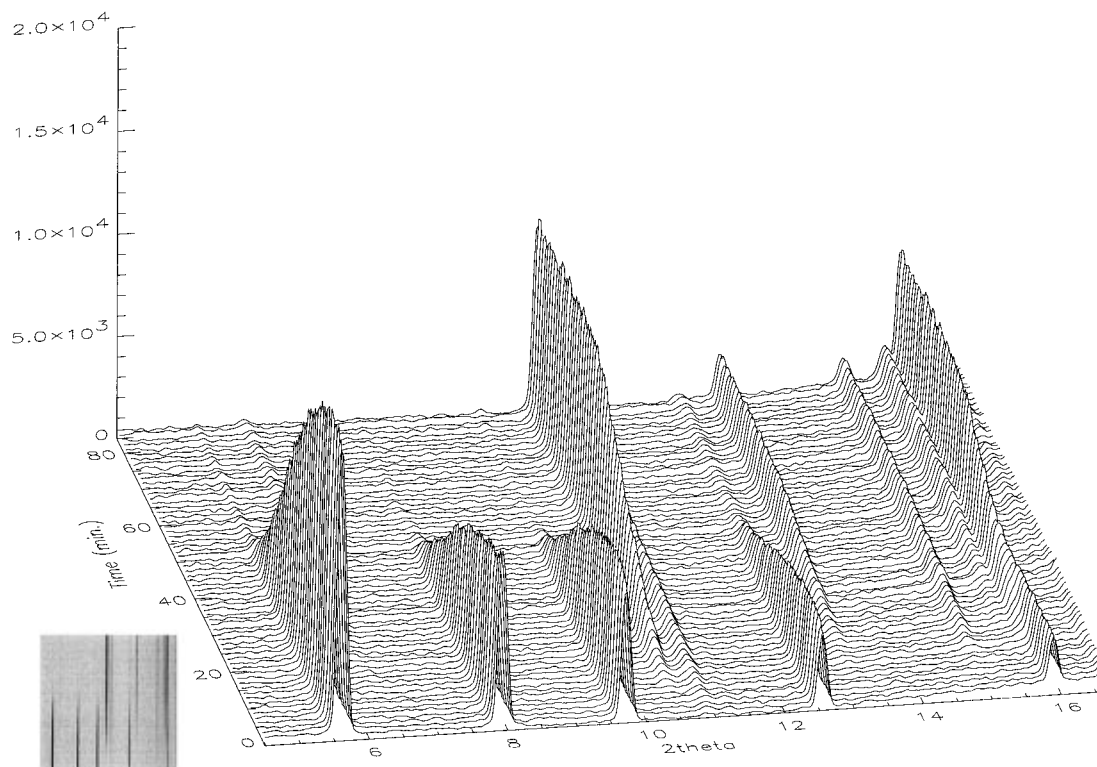
Figure 4. 3-Dimensional plot of powder diffraction profiles as a function of time during the hydrothermal conversion of zeolite Li/Na-LTA to zeolite Li-A(BW). The wavelength used was 1.1727(2) Å. The temperature was ramped to 200 °C in 5 min and kept at that temperature.

solution of LiCl. In this experiment the sample was heated to 260 °C in 1 h and kept at that temperature for 1 h. The product is a mixture of two phases. The main product is zeolite Li-A(BW), but a small amount of another phase is also present, indicated in Figure 3a. The diffraction peaks from this phase could be indexed with a hexagonal unit cell: $a = 12.419(8)$ Å and $c = 5.003(8)$ Å, which is in agreement with a cancrinite-type phase.

Diffraction lines from undissolved LiCl are present in the beginning, but disappear at higher temperatures as the salt dissolves. Figure 3b is an enlargement of a small portion of the image at higher diffraction angles. It is evident that just before the transformation an expansion of the unit cell takes place. This expansion was observed only in the hydrothermal conversion experiments performed at 260 °C. The cubic unit cell parameter of zeolite LTA increases abruptly from 12.090(4) to 12.135(2) Å. (The unit cell parameters were refined by using the subcell of the zeolite LTA unit cell.) In comparison, the unit cell parameter for zeolite LTA in the experiment at 180 °C only increases from 12.053(1) to 12.063(2) Å before conversion takes place. The difference between the two samples is that the starting material for the 180 °C experiment was ion exchanged with Li beforehand, and there is therefore a significant difference in the concentration of Na cations in the two experiments. For comparison, the unit cell parameter of hydrated zeolite LTA at room temperature is 12.30 Å for the Na form and ~12.04 Å for the Li ion exchanged form. As seen from the lattice constants, the zeolites in both experiments are initially partially Li ion exchanged. However, the increase in the unit cell parameter is significantly larger for the experiment with the highest concentration of Na cations.

(21) Barrer, R. M.; Cole, J. F.; Villiger, H. *J. Chem. Soc. (A)* **1970,** 1523–1531.

(22) Colella, C.; de'Gennaro, M. In Zeolite Synthesis; ACS Symp. No. 398; American Chemical Society: Washington, DC, 1989, p 196.

(23) Norby, P.; Krogh Andersen, I. G.; Krogh Andersen, E.; Colella, C.; de'Gennaro, M. *Zeolites* **1991,** *11,* 248–253.
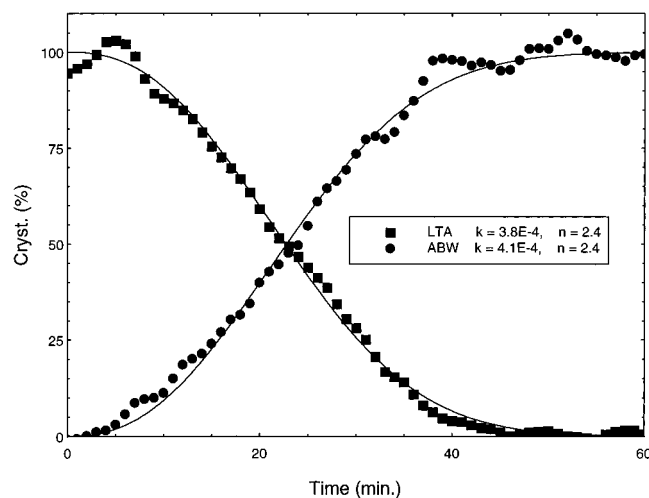
Figure 5. Crystallization and degradation curves for zeolite Li-A(BW) and Li/Na-LTA, respectively, corresponding to a hydrothermal conversion experiment performed by ramping the temperature to 180 °C in 5 min and holding the temperature constant. The amount of crystalline material was estimated by using integrated intensities of diffraction lines. Fitted crystallization curves from the Avrami equation are shown (solid lines), see text.

The unit cell expansion could be caused by either a shift in the ion exchange equilibrium, causing an increase of the sodium content in the zeolite, or an increase in the hydration level of the zeolite as the temperature is increased.

Figure 4 is a 3-dimensional representation of the diffraction profiles as a function of time during hydrothermal conversion of zeolite LTA in LiCl$_{(aq)}$. The sample was heated to 200 °C in 2 min, and kept at that temperature. The degradation of zeolite LTA and the simultaneous formation of zeolite Li-A(BW) are clearly visible. In the low-angle region it is evident that the intensities of several of the reflections from zeolite LTA increase to a maximum before decreasing. This increase is

correlated with the slight increase in the unit cell parameters mentioned above. The intensity changes could therefore be related to structural changes caused by ion exchange or by changes in the hydration level of the zeolite. The analysis of crystallization kinetics is difficult if significant structural changes take place before or during the transformation. One of the assumptions for using integrated intensities of diffraction lines as a measure of the amount of crystalline material is that changes in the intensity are solely caused by decrease in the amount of crystalline material and not by structural changes.

Discussion

Several possibilities exist for the transformation mechanism during hydrothermal conversion from zeolite LTA to Li-A(BW). Some possible mechanisms are the following:

(1) internal structural transformation [rearrangement of the framework with retention of the crystal morphology; nucleation will occur at a point in the crystal and spread throughout the crystal; no intermediate amorphous or solution phases are active in the process], (2) gel-mediated transformation [partial or complete transformation of the starting material into an amorphous phase and subsequent nucleation and crystallization of the new phase], (3) solution-mediated transformation [partial or complete dissolution of the starting material followed by nucleation and crystallization of the new phase], (4) surface-mediated transformation [migration of ions along the crystals of the starting material; nucleation occurs on the crystals of the starting material, and no preservation of crystal morphology is necessary], and (5) structural similarity enhanced transformation or epitaxial crystallization [nucleation and crystal growth occur at crystal faces with structural features common to the starting material and the product; this type of crystallization could be mediated by partial dissolution or amorphization, as well as by migration].

Crystallization and degradation curves were extracted by using integrated intensities of a number of diffraction lines from the product and the starting material, respectively. The progress of the hydrothermal conversion can be followed and compared to models, which allows information concerning kinetics and transformation/crystallization mechanisms to be extracted.

Figure 5 shows results from a hydrothermal conversion experiment performed at 180 °C. In the figure normalized integrated intensities of diffraction lines from the starting material, zeolite LTA, and the product, zeolite Li-A(BW), are plotted as a function of time. The conversion curves have typical sigmoidal shapes, and the crystallization curve for zeolite Li-A(BW) and the degradation curve for zeolite LTA cross close to 50% conversion. This implies that no amorphous or solution phases are present to any great extent. If significant amounts of the starting material had been dissolved or transformed into amorphous material, the conversion curves would cross below 50% crystallinity. Also, no apparent loss of crystallinity of zeolite LTA was observed. Profile fitting showed that the full width at half maximum (fwhm) of reflections for zeolite LTA was almost constant during the conversion. If significant amounts of defects, disorder, or strain were introduced, line broadening would be observed correlated with the decrease of percent of crystalline material. The lack of line broadening effects implies that only the surface of the crystals is dissolved, while the integrity of the structure is retained.

The crystallization curve was fitted with the Avrami equation:[3,24]

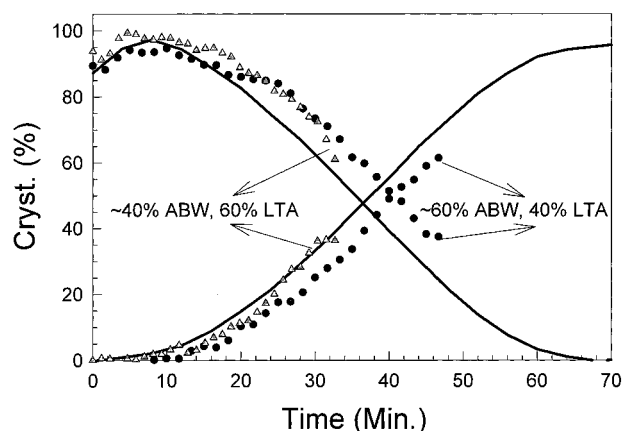(24) Thompson, R. W.; Dyer, A. *Zeolites* **1985**, *5*, 202−210.

Figure 6. Crystallization curves for three experiments at 200 °C (temperature ramp 5 min). The solid line shows the complete conversion to zeolite Li-A(BW), while the other curves represent preparation of partially converted samples. The samples were quenched after 30 and 45 min, respectively, and the final conversions were estimated to approximately 40% (sample 1, triangles) and 60% (sample 2, filled circles) for the two samples.

$$I(\%) = 100(1 - \exp(-k(t - t_0)^n))$$

and a similar equation for the degradation of zeolite LTA:

$$I(\%) = 100 \exp(-k(t - t_0)^n)$$

k is the rate constant and t_0 is the time when crystallization starts. In Figure 5 the curves obtained from the fit to the Avrami equation are shown. A reasonable fit is obtained for both curves. The derived values for the rate constants, k, are similar for the degradation and crystallization curves, and the value of n found was 2.4 for both curves. t_0 was fixed to be zero, as the conversion starts as soon as the final temperature is reached.

In kinetic studies of zeolite crystallization the value of n in the Avrami equation is 4 for constant linear growth rate and a constant nucleation rate.[2,24] However, values of n are often found to be significantly greater than 4, especially when the starting materials are gels or amorphous metakaolinites.[10] This has been attributed to an autocatalytic nucleation effect. The value of n is expected to be less than 4 also when the morphology of the growing crystal is far from cubic, which means that the linear growth rates are very different for each crystallographic direction. The typical morphology of zeolite Li-A(BW) crystals is flat needles.[1] Other factors, such as limited nucleation, may also result in lower values of n.

From the crystallization curves some information about the crystallization mechanism can be extracted, although a conclusive analysis is not possible. It is obvious from the curves that the crystallization does not involve formation of significant amounts of amorphous phases or dissolved material. Also, the analysis clearly indicates that no autocatalytic nucleation is occurring, and is indicative of a limited nucleation rate. Considering the low pH (∼8) of the solution, it is reasonable to assume that the solubility of aluminosilicate species is small. The low surface area of the starting material as compared to amorphous aluminosilicate gels will also limit the rate of dissolution. The low value obtained for n is in agreement with a crystallization process where only minor amounts of material go into solution and where the zeolite crystals grow from a limited number of nucleation sites.

To further investigate the transformation mechanism, controlled partial conversion experiments were performed *in situ* on the diffractometer. The temperature selected was 200 °C.
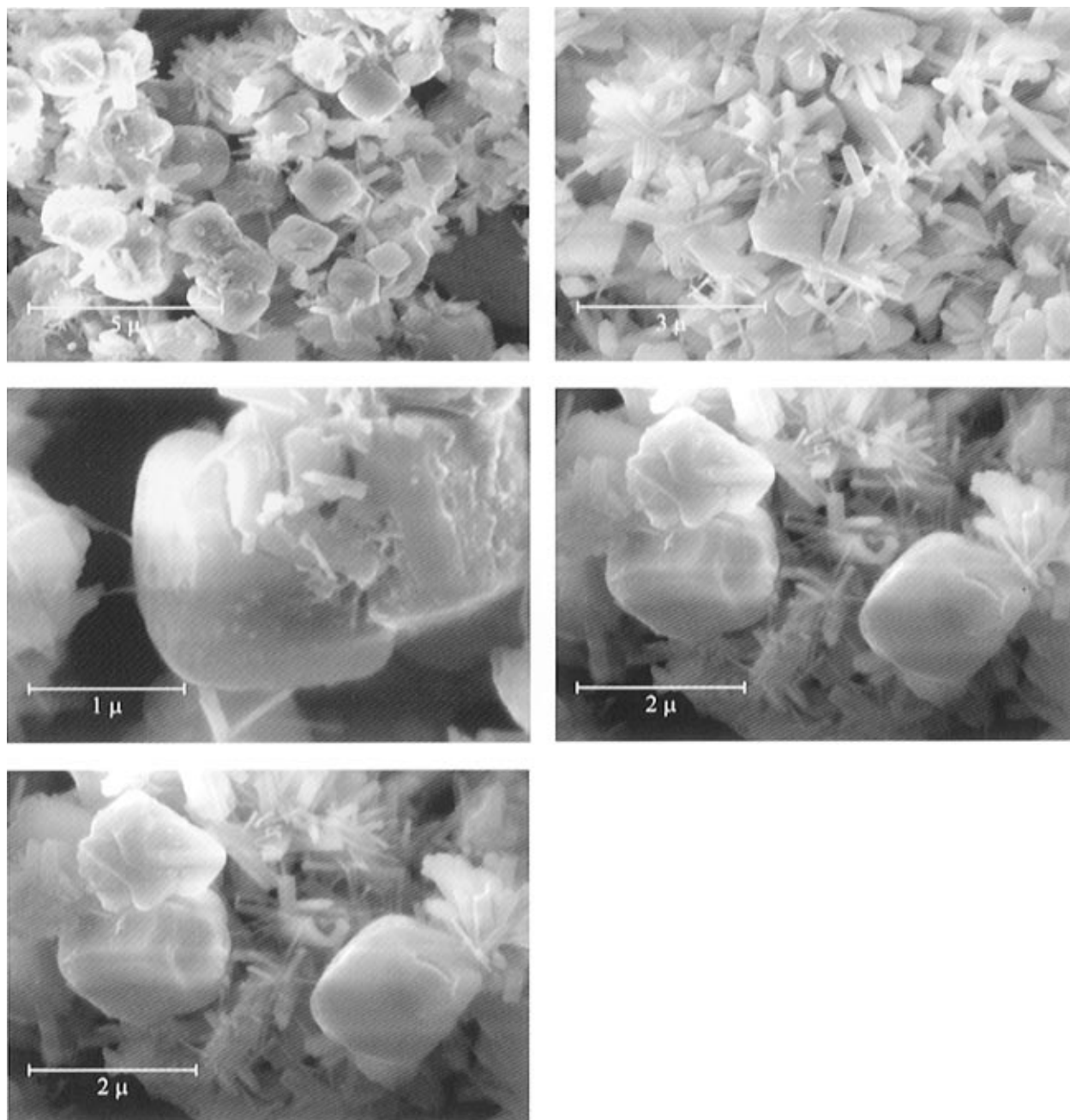
Figure 7. Scanning electron micrographs of the partially converted samples. (a, top left) Overview of sample 1, the 40% converted material. Etched cubic LTA crystals are seen together with clusters of radially growing needles of ABW crystals. (b, top right) Overview of sample 2, 60% conversion. A mixture of LTA and ABW crystals. The LTA crystals are severely etched and the cubic morphology of the crystals is no longer apparent. Zeolite Li-A(BW) crystals are seen in pronounced radially growing clusters. (c, middle left) Etching of LTA intergrown crystals with scattered crystals of zeolite Li-A(BW). (d, middle right) Severely etched LTA crystals with clusters of zeolite Li-A(BW) in the background. Clusters of ABW crystals are growing on edges and interfaces of LTA crystals. (e, bottom) Well-formed LTA crystals and several groups of Li-A(BW) crystals. Some clusters consist of radially growing crystals, which are very thin compared to the majority of the Li-A(BW) crystals.

At this temperature the transformation is slow enough to attempt to control the degree of conversion, and at the same time the temperature is high enough to get highly crystalline zeolite Li-A(BW).

Figure 6 shows crystallization curves for *in situ* hydrothermal conversion of Li-exchanged LTA in an aqueous solution of LiCl. The temperature was raised to 200 °C in 5 min and kept at that temperature. The only product observed was zeolite Li-A(BW), and conversion was complete after ca. 70 min.

Partially converted samples were prepared by stopping the experiment after 30 and 45 min, respectively. These experiments were also followed by using time resolved powder diffraction in order to estimate the degree of conversion. The corresponding crystallization curves are shown in Figure 6. The

percent crystallinity for zeolite Li-A(BW) in the two samples was estimated by scaling the crystallization curve so that the final crystallinities added up to 100%. The two samples had an estimated content of 40% and 60% zeolite Li-A(BW), respectively.

SEM pictures of the two samples are shown in Figure 7a−e. Several features should be noted.

(1) The crystal morphologies of the two zeolites are very different. The LTA crystals have the well-known cubic appearance (Figure 7a,c,d), although the edges have been smoothed compared to the starting material. The Li-A(BW) crystals grow as needles as also described e.g. in ref 1.

(2) The zeolite Li-A(BW) crystals grow in radial clusters, and the nucleation centers are not independent of the starting

material. Nucleation starts at the zeolite LTA crystal surface. Especially micrographs a and d in Figure 7 indicate that nucleation starts at corners and faults of the LTA crystals, where chemical and structural strain is significant. In Figure 7b very well developed radial clusters of zeolite Li-A(BW) crystals can be seen.

(3) The LTA crystals show signs of etching, which becomes more visible as the conversion progresses. Figure 7c shows etching pits on the surface of one of the LTA crystals, and Figure 7d shows the deformation and rounding of several crystals. Figure7b shows an overview of part of sample 2 where ca. 60% conversion has taken place. The well-developed faces of the LTA crystals have almost completely disappeared as a result of the etching of the crystals. Although the material looks almost amorphous, it is important to note that there is no significant amount of amorphous material present.

(4) The majority of the crystals of zeolite Li-A(BW) have similar sizes. The crystals grow radially from a limited number of nucleation sites. However, there are a few clusters of crystals of much smaller size, seen especially in Figure 7e. Radially growing clusters of crystals are often found for both synthetic and naturally occurring zeolites.

Combining the information from the *in situ* powder diffraction experiments and the *ex situ* SEM investigations allows the conclusion that the hydrothermal conversion of zeolite LTA into zeolite Li-A(BW) in LiCl$_{(aq)}$ is a solution-mediated process, with only very small amounts of the aluminosilicate in solution. The LTA crystals lose their distinct cubic morphology and in the later stages of conversion do not have a crystalline appearance when observed in the electron microscope. However, the diffraction experiments clearly show that there is no formation of amorphous phases as the crystallization progresses. The parent zeolite LTA crystals serve as nucleation sites for the radially growing clusters of zeolite Li-A(BW) crystals, and nucleation on edges and interfaces of the crystals is common. Nonetheless, there is no indication of an epitaxial nucleation and crystal growth. The crystals grow mainly in radially extending clusters with no obvious correlation to the crystal structure of the zeolite LTA crystallites. There is a limited number of nucleation sites, and growth on primary nucleation sites seems to be predominant.